

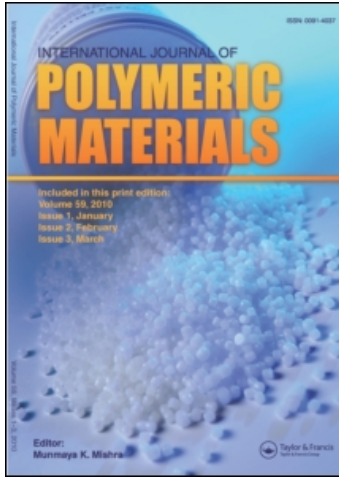
This article was downloaded by:

On: 23 January 2011

Access details: *Access Details: Free Access*

Publisher *Taylor & Francis*

Informa Ltd Registered in England and Wales Registered Number: 1072954 Registered office: Mortimer House, 37-41 Mortimer Street, London W1T 3JH, UK



## International Journal of Polymeric Materials

Publication details, including instructions for authors and subscription information:

<http://www.informaworld.com/smpp/title~content=t713647664>

### Aspects of the Calendering of Plastics Compositions

B. S. Glyde<sup>a</sup>

<sup>a</sup> Bakelite Xylonite Limited, Cascelloid Division, Leicester

**To cite this Article** Glyde, B. S.(1977) 'Aspects of the Calendering of Plastics Compositions', International Journal of Polymeric Materials, 5: 4, 271 – 289

**To link to this Article:** DOI: 10.1080/00914037708075211

**URL:** <http://dx.doi.org/10.1080/00914037708075211>

PLEASE SCROLL DOWN FOR ARTICLE

Full terms and conditions of use: <http://www.informaworld.com/terms-and-conditions-of-access.pdf>

This article may be used for research, teaching and private study purposes. Any substantial or systematic reproduction, re-distribution, re-selling, loan or sub-licensing, systematic supply or distribution in any form to anyone is expressly forbidden.

The publisher does not give any warranty express or implied or make any representation that the contents will be complete or accurate or up to date. The accuracy of any instructions, formulae and drug doses should be independently verified with primary sources. The publisher shall not be liable for any loss, actions, claims, proceedings, demand or costs or damages whatsoever or howsoever caused arising directly or indirectly in connection with or arising out of the use of this material.

# Aspects of the Calendering of Plastics Compositions

B. S. GLYDE

*Bakelite Xylonite Limited, Cascelloid Division, Leicester*

*(Received September 30, 1976)*

Pressure distribution curves derived from isothermal power-law theory are shown to match closely with the experimental data of Bergen and Scott. A method of estimating roll bearing loads from torque measurements obviates errors incurred when using plastometry. An analysis of unequal roll speed calendering is presented and surface pattern formation is explained as a laminar flow effect, with experimental evidence.

## INTRODUCTION

Calendering is a means of forming a sheet by passing a mass of plastic material between rollers. The process has been analysed in remarkably few publications although it is widely employed in industry, particularly in the manufacture of floor and wall coverings.

Ardichvili<sup>1</sup> in 1938 and Eley<sup>2</sup> in 1946 arrived at similar expressions for the pressure distribution between the rolls; they considered the deformation of the material as a homogeneous compression, and assumed that the material would leave the rolls at the nip. The first treatment based on a viscous flow model was that of Gaskell<sup>3</sup> in 1950 who derived equations relating to Newtonian fluids as well as the pressure distribution function for a general non-Newtonian fluid. Using a Bingham plastic as an example he showed that the sheet should leave the rolls at a thickness greater than that of the nip. Publishing in 1951 Atkinson and Nancarrow<sup>4</sup> pioneered the use of a plunger rheometer, recognized the wide applicability of the power-law flow function to thermoplastics and applied it to several processes including calendering.

Bergen and Scott<sup>5</sup> determined pressure profiles using a transducer in the roll surface and provided support for Gaskell's conclusions, although they experienced difficulty in matching the empirical and theoretical pressure profiles. Dexter and Marshall<sup>6</sup> calculated roll separation forces using Ardichvili's

equations together with some of Gaskell's concepts and claimed reasonable quantitative agreement between theory and practice. Paslay<sup>7</sup> extended Gaskell's viscous flow solution to include elasticity on a Maxwell model, showing the effect of relaxation time on pressure gradient, but did not consider elastic recovery at the point where the material leaves the rolls.

The work presented here was carried out mainly between 1955 and 1958. The author wishes to acknowledge the contribution made in 1962 by a colleague, B. Martin, who used a computer to produce numerical solutions to the differential equations. McKelvey<sup>8</sup> in 1962 and Pearson<sup>9</sup> in 1966 further developed the analyses for Newtonian and power-law fluids, introducing some mathematical rigour and thus saving the present author from justifying his assumptions, since the model used is basically the same as that of the previous workers<sup>3,4,8,9</sup> mentioned.

### Special features of the process

A calender is justifiably called a press because it does virtually the same job as a platen press but in a continuous manner. The vertical bearing loads are very high, but there is little or no horizontal load because the horizontal component of pressure on the roll surface is balanced by the surface shear stress.

It is a basic characteristic of the process that when the roll speeds are equal the extruded sheet tends to leave the rolls with every part of the mass at the same velocity, so that the sharkskin effect encountered in extrusion through fixed dies is absent. Even a slight thickness reduction makes it possible to "put a finish" onto a sheet; the surface suffers blemishes only when excessive adhesion to the roll surface prevents a clean break at exit. A calender can produce a hard, smooth sheet from a highly-filled mix containing only 20–30% of polymer binder. By contrast, when such a material is extruded through a cylindrical die the extrudate breaks up into a series of hollow cones because the forces involved in equalizing the exit speed exceed the cohesive strength of the material. This is a pronounced version of the sharkskin effect observed when extruding less rigid materials.

In sufficiently slow calendaring elastic recovery effects (analogous to die swell) in the extrudate are absent because the shear rate is zero at exit. In faster calendaring the extrudate may retain the memory of shear experienced before and after the pressure maximum, causing the sheet to leave the rolls at a thickness greater than that predicted by viscous flow theory. Melt fracture is not experienced even at high speeds because there are no rapid changes in the shape of the flow channel; shear acceleration is therefore relatively slow and the structure of the polymer melt is able to comply at the required rate.

If different roll speeds are used the sheet tends to cling to the faster roll because the normal stress differential creates a greater tension on that side of

the sheet when leaving the nip. The normal stress effect may be masked by the existence of a temperature differential between the rolls; some polymers stick more firmly to a colder surface, others to a hotter one.

The feed material rarely sticks to the roll surfaces immediately on entry (see Figure 12); there is normally a short distance over which the material skids until it picks up enough friction to build up pressure, which then effects adhesion. If one roll is much hotter than the other, the mass may slip against that roll throughout, giving rise to considerably distorted velocity profiles.

Various surface patterns can be produced, entirely as a result of laminar flow, by using different roll speeds and temperatures together with special pre-form preparation using multi-coloured feedstock. Some of these patterns are similar in type to effects which can be produced by extrusion and injection moulding.

### Theory: Assumptions of the model

The simplifying assumptions made in this treatment do not differ from those of Gaskell, McKelvey and Pearson, and have been dealt with comprehensively by these authors. The process is treated as if it were isothermal, and the roll dimensions are assumed to be large compared with the arc of contact. The calendered material is assumed inelastic.

The material being calendered is regarded as a power-law pseudoplastic having a basic flow equation

$$\dot{\gamma} =: \phi \sigma^\nu \quad (1)$$

where  $\dot{\gamma}$  is the shear rate,  $\sigma$  the shear stress and  $\phi$  the fluidity (or reciprocal viscosity) at unit shear stress. The exponent  $\nu$  is assumed to be an odd number, because the use of an "odd" function  $F(-x) = -F(x)$  avoids the necessity for complicating the equations with instructions about signs. An even exponent can always be approximated by the ratio of two large odd numbers.

### PRESSURE FUNCTION

A derivative of the velocity distribution and pressure equations from the geometry of Figure 1 for equal speed rolls is given in Appendix A. These equations have appeared in other papers<sup>3,8,9</sup> in one form or another. Successive integration of the flow equation with appropriate limits leads to the expression

$$\phi G^\nu h^{\nu+2} = U (h - h_e) (\nu + 2) \quad (2)$$

where  $G$  is the pressure gradient  $dp/dz$  in the flow direction. It has been assumed the the sheet leaves the rolls at the peripheral speed, so that the flow rate is  $2LUh_e$ .

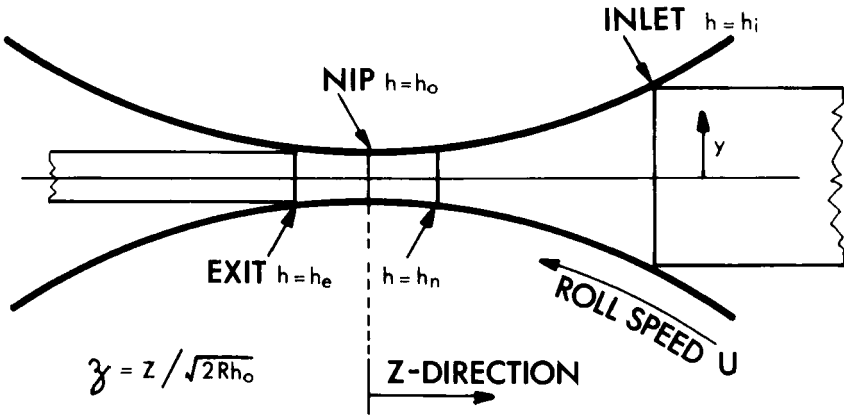


FIGURE 1 Geometry of the equal roll speed treatment.

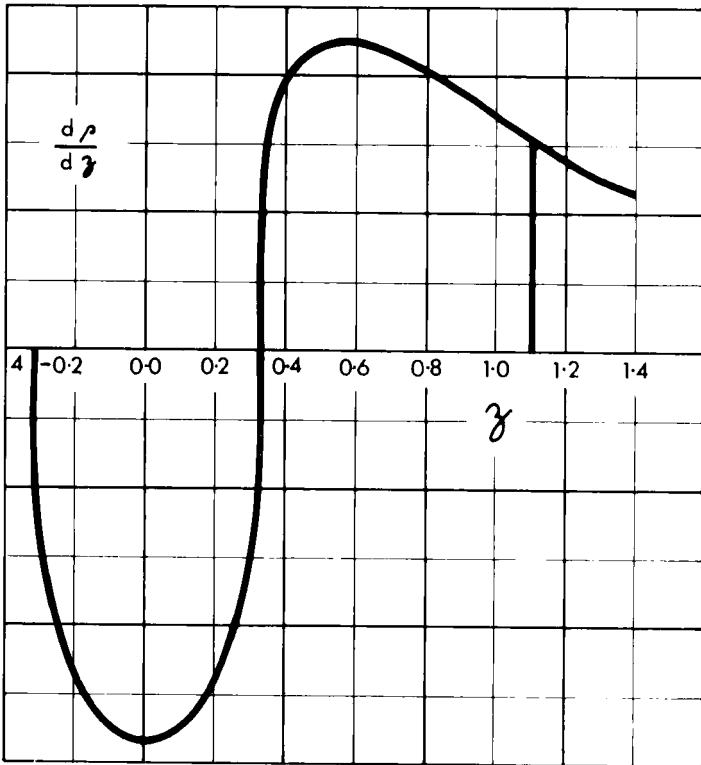


FIGURE 2 Pressure gradient curve for  $v = 4$ ,  $h_n = 0.32$ .

To a first approximation the gap between the rolls can be related to distance from the nip by the equation  $h/h_0 = 1 + \zeta^{2\ddagger}$  where  $\zeta = z/\sqrt{2Rh_0}$ . A typical pressure gradient curve is shown in Figure 2. Equation (2) can be integrated in the form

$$p = K_1 \int_{\zeta_i}^{\zeta} F(\zeta) d\zeta \quad (3)$$

where  $\zeta_i$  is the entry point where  $p = 0$ . The material will leave the rolls where  $p = 0$  again, i.e. where

$$\int_{\zeta_i}^{\zeta_e} F(\zeta) d\zeta = 0 \quad (4)$$

It can be shown that  $\zeta_e = -\zeta_n$  where  $\zeta_n$  is the position of maximum pressure, and that the pressure at the nip is half the maximum pressure. Thus  $h_e = h_n$ .

Bergen and Scott<sup>5</sup> made measurements of pressure using a transducer in the roll surface. The result of one experiment is shown as curve (a) in Figure 3. In comparing their results with Gaskell's Newtonian theory the curves were matched at the nip, and the  $\zeta$  values at the point of maximum pressure were made to coincide, so that a very bad fit was obtained in the entry region. Moreover, the filled thermoplastic used was clearly non-Newtonian and although comprehensive flow data are not available it is clear from Figure 3 that the power-law-based pressure profile (c) with  $\nu = 4$  can be made to give a much better fit. Even their Newtonian curve (b) can be made to fit better (curve (d)) if some licence is taken on the position of  $\zeta_e$ . The best fit would be achieved by  $\nu = 7+$ , but such values are not supported by experiments on filled thermoplastics which normally have  $\nu$  values between 2 and 4.

The most likely explanation for the more gradual rise of pressure at the inlet in the experiment is suggested by the familiar experience that the entering sheet or bank of feed material slips against the rolls until enough pressure is built up for full adhesion.

The insensitivity of  $h_n$  to  $h_i$  is shown by Figure 4 plotted from Eq. (4). It is clear that the  $h_n - h_i$  curves and hence the  $\zeta_n - \zeta_i$  curves are very close together over a wide range of  $\nu$  values. Figure 5 shows  $h_i/h_n$  plotted against  $h_i/h_0$ .

## BEARING LOADS AND DRIVING POWER

By integrating pressure and shear stress separately over the arc of contact (Appendix B) expressions can be obtained for the total load on the roll bearings and the torque required to drive the rolls. Taking the ratio of these quantities eliminates the specific fluidity  $\phi$  and thus removes an important source of

†Zeta drawn as a zed on the figures.

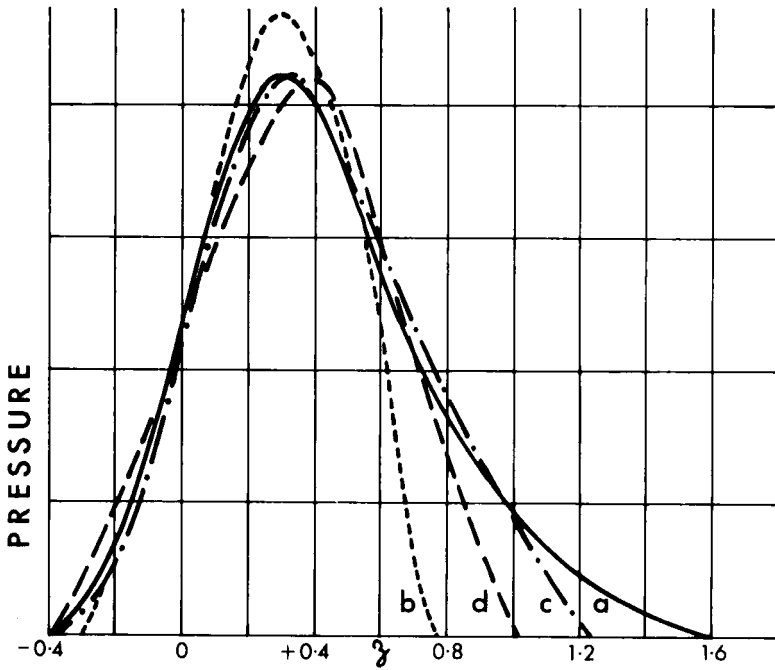


FIGURE 3 Comparisons of Bergen and Scott data with theory (see text p. 275).

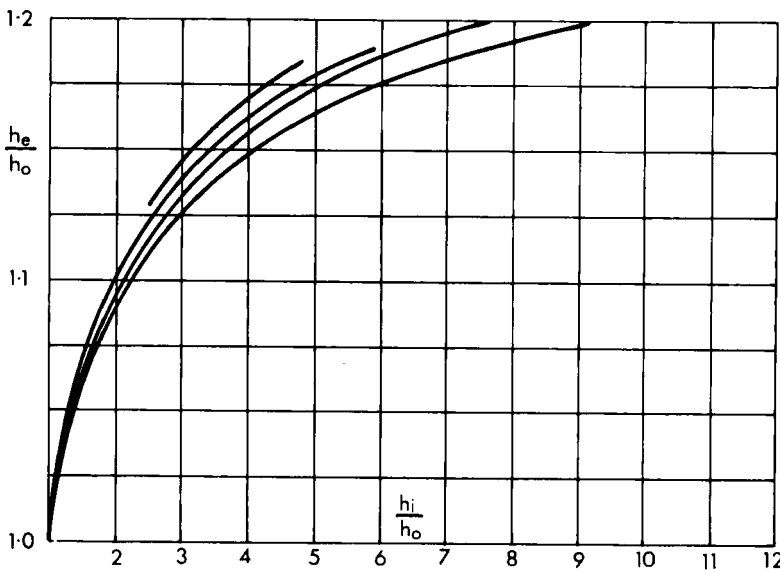


FIGURE 4 Inlet versus exit thickness related to nip gap. From lower curve  $\nu = 7$ , others are for  $\nu = 4, 3$  and  $2$ .

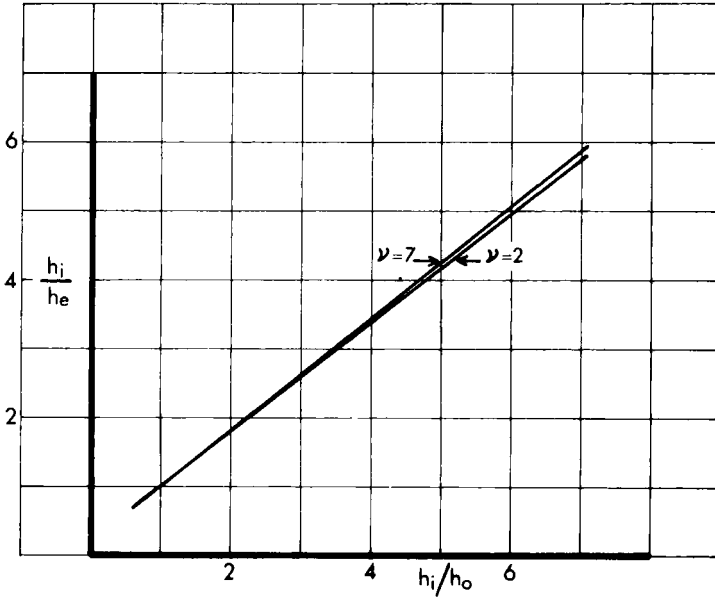


FIGURE 5 Plot of inlet-exit thickness ratio against inlet-nip ratio.

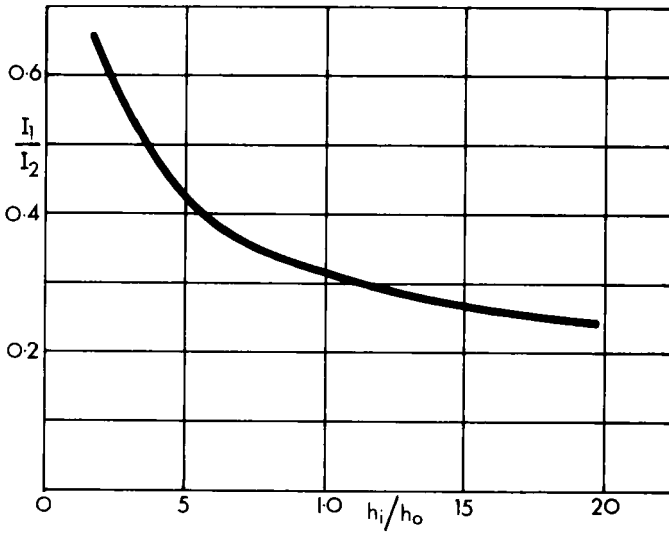


FIGURE 6 Ratio of integrals for bearing load-drive power ratio.

error which is unavoidable when calculating bearing loads from e.g. Eq. (3) with data obtained from plastometry. Errors due to non-isothermal conditions and to slip in the entry region will also be reduced. The exponent  $\nu$  can usually be estimated more accurately. For calender design purposes measurements on one calender can easily be translated for other sets of dimensions and conditions.

$$\frac{\text{Load on each end of the rolls}}{\text{Drive power}} = \frac{U}{\sqrt{2h_0}} \cdot \frac{I_1}{I_2}$$

which is another form of Eq. (16) in Appendix B.

The integrals  $I_1$  and  $I_2$  are derived in Appendix B and a typical  $I_1/I_2$  curve is shown in Figure 6.

## UNEQUAL ROLL SPEEDS

In published work<sup>9</sup> the flow analysis for the case of unequal roll speeds has not been taken further than a statement of the velocity distribution equation, except in the case of the Newtonian fluid where unequal speeds do not give rise to complication.

The derivation of the pressure gradient function is given in Appendix B. By considering a datum line  $y = 0$  where shear stress is zero the flows on each side of the line can be compared, matching the flow velocity at the line, which is shown dashed in Figure 7. Approximate shapes of velocity profiles in each region are also shown. Where the datum lies inside the roll there is no velocity minimum or maximum within the flowing mass.

The pressure gradient can then be expressed as a function of  $h$  (and thus as a function of  $\zeta$ ) via parametric equations in  $\lambda$  ( $h_1/h_2$ , the ratio of distances from the datum line to the faster and slower rolls respectively). The ratio  $\rho$  of the speed  $U_1$  of the faster roll to the speed  $U_2$  of the slower roll is also used.

The pressure gradient  $G$  at a point where the gap between the rolls is  $2h$  is given by (Appendix C Eq. (22))

$$\frac{\phi G^\nu h_n^{\nu+1}}{2U(\nu+1)} = \frac{\rho-1}{\rho+1} \cdot \frac{(\lambda+1)^{\nu+1}}{\lambda^{\nu+1}-1} \cdot \left(\frac{h_n}{2h}\right)^{\nu+1} \quad (5)$$

where

$$\frac{h_n}{2h} = \frac{1}{\rho+1} + \frac{\rho-1}{\rho+1} \left[ \frac{\lambda/(\lambda+1) - (\nu+1)/(\lambda^{\nu+1}-1)}{\nu+2} \right]$$

Pressure gradient curves calculated from Eq. (5) are shown in Figure 8 and pressure distribution in Figure 9. One problem is that when  $\rho$  is significantly larger than unity the shapes of the pressure curves are very different from those obtained in the case of equal roll speeds, and no check is possible by putting

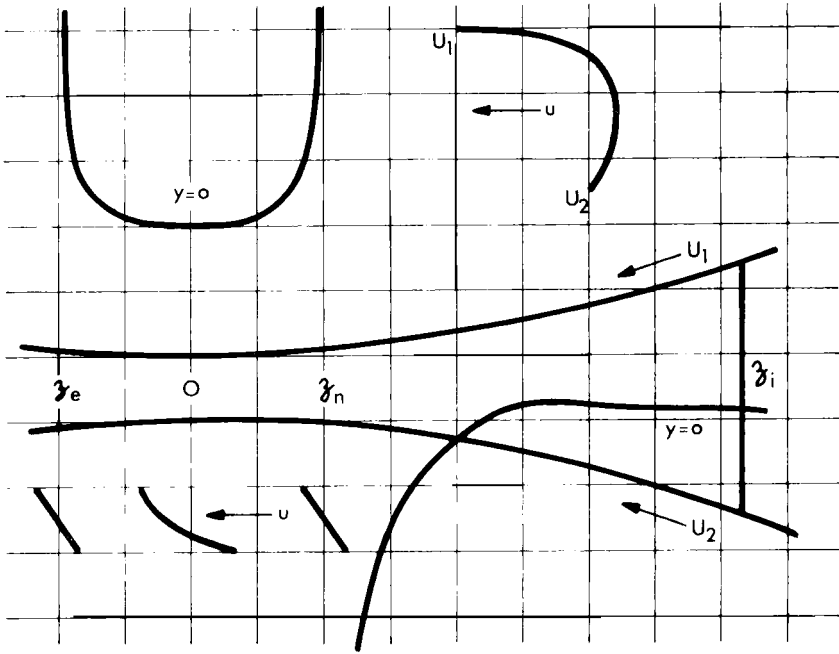


FIGURE 7 Geometry of the unequal roll-speed treatment.

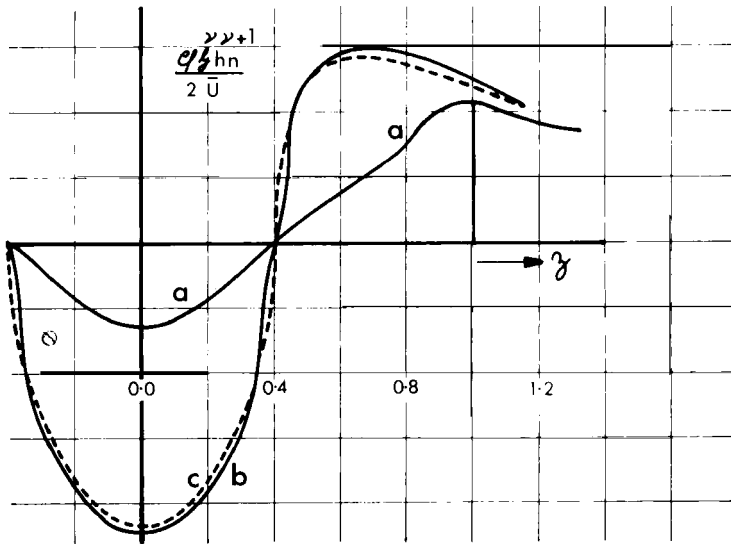


FIGURE 8 Pressure gradient curves for unequal roll speeds,  $\nu = 3$ . (a)  $\rho = 3$ , (b)  $\rho = 1.1$ , (c) (dashed)  $\rho = 1$ .

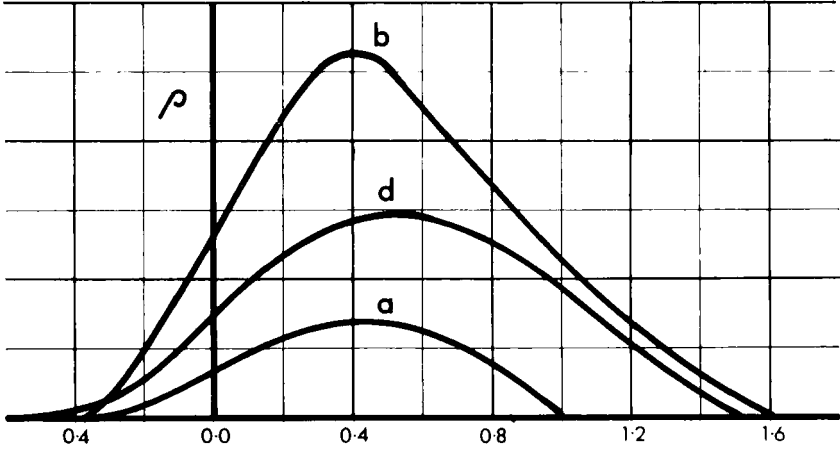


FIGURE 9 Pressure distributions for (a)  $\rho = 3, h_n = 0.4$ , (b)  $\rho = 1.1, h_n = 0.4$ , (c)  $\rho = 3, h_n = 0.5, \nu = 3$ .

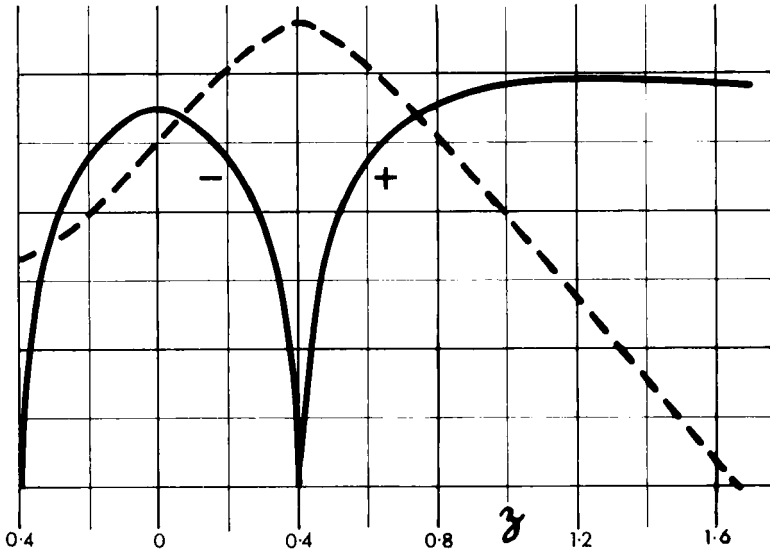


FIGURE 10 Shear rate at roll surface versus  $\zeta$ .  $U_1 = U_2$  and  $\nu = 3, h_n = 0.4$ . Negative and positive shear rates have been plotted on the same side of the  $\zeta$ -axis.

$\rho = 1$  since the derivation depends on  $\rho \neq 1$ . This difficulty is overcome by accurately plotting curves for a value of  $\rho$  slightly greater than unity (curve (b), Figure 8 shows  $\rho = 1.01$ ) showing that there is a rapid transition from a more pointed to a more rounded pressure profile over a small range of speed ratio. The "pointedness" is controlled by the shape of the  $dp/dz$  curve at  $\zeta_n$  (Figure 8).

As shown in Figures 8 and 9 the pressure maximum is at  $\zeta = \zeta_n$ . As with the case of equal roll speeds the pressure at the nip ( $h_0$ ) is half the maximum pressure, and the extrudate leaves the rolls at  $\zeta = -\zeta_n$ , however different the roll speeds. These properties are hardly surprising since they result directly from the symmetry of the flow channel around the nip. As  $\rho$  is increased to 3 the change in the shape of the pressure profile compared with that of  $\rho = 1$  becomes dramatic,  $dp^2/dz^2$  being almost exactly halved over a wide range of  $\zeta$ . When one roll is stopped altogether the value is reduced to less than one fifth in the region of  $\zeta_n$ . Unfortunately, it is not possible to see the real effect of speed differential on bearing load from comparing pressures at similar  $\zeta_n$  values, because the  $\zeta_n - \zeta_1$  relationship changes with  $\rho$ . We have not yet programmed a computer to find  $\zeta_n$  values for different  $\rho$  at the same inlet thickness.

At the point  $\zeta_n$  the shear rate is zero for all  $y$  when roll speeds are equal, and constant at  $\dot{\gamma}_n = (U_1 - U_2)/2h$  when  $U_1$  and  $U_2$  are unequal. On the inlet side of  $\zeta_n$  the material is travelling more slowly than the mean roll speed. On the exit side it travels increasingly faster up to the nip and then slows down until its average speed is equal to that of the rolls at exit.

It should be noted that the mean velocity of the issuing sheet cannot equal the surface speed of either roll. The surface which leaves the slower roll is impaired due to the dragging effect. In practice the sheet will often stick to the faster roll, and particularly so if the temperature of that roll is more suited to adhesion. This effect is often used to advantage in take-off systems.

## SURFACE PATTERN EFFECTS

Calendered sheets used for decorative purposes are often self-coloured and bear various types of distinctive surface pattern such as streaky or marbled effects. These patterns are due entirely to laminar flow in the plastic components of the mix and depend on

- i) the striation thickness of components of different colour at the surface of the sheet
- ii) the size of filler particles relative to the striation thickness
- iii) the initial size, shape and orientation of particles of various coloured components in the feed material

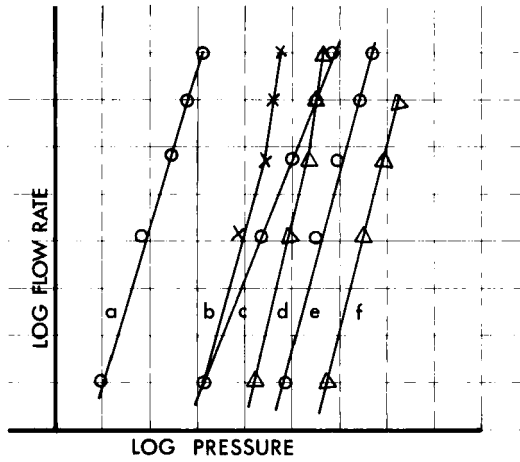


FIGURE 11 Log log plot of pressure versus flow rate in Atkinson-Nancarrow plastometer.

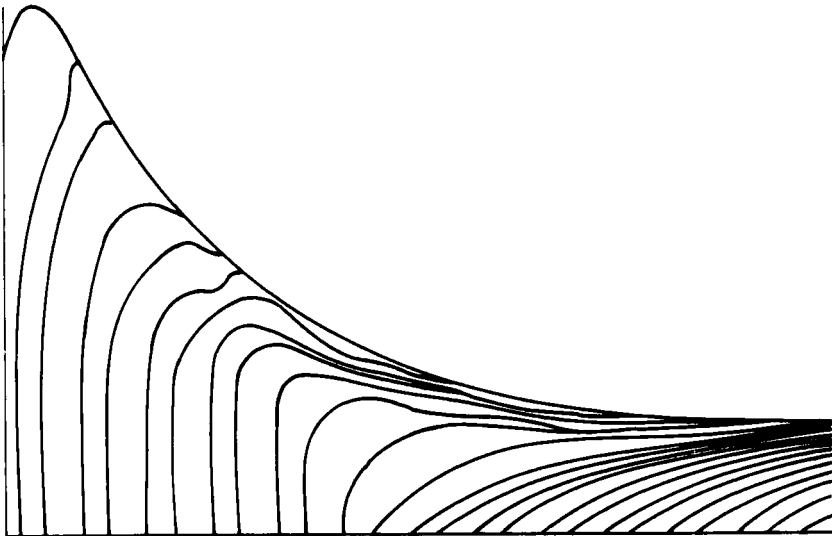


FIGURE 12 Striations ("strain profiles") formed by calendering a striped sheet.

The striation thickness of a component is inversely proportional to the amount of shear incurred during passage through the calender. The amounts of shear experienced by the different components are determined by the ratios of their viscosities. Effects such as streaking or marbling will not appear until the total shear is enough either to lengthen the original streaks of coloured material sufficiently or, in the case of marbling, to reduce the striation thickness to such an extent as to enable one layer to break through another at the surface; this effect can be modified by the presence of particles of filler larger in diameter than the striation thickness.

Patterns are thus usually formed at the surface of the faster roll where the shear rate is higher. Different roll temperatures can be used either alternatively or as a complement to different speeds. Most of the unrecoverable shear is experienced before the pressure maximum is reached at  $\zeta_n$ ; changes in shear rate experienced between  $\zeta_n$  and  $\zeta_0$  are reversed again between  $\zeta_0$  and  $\zeta_e$ . It would be wrong to assume that there is no further development of the pattern, since all striation breakthrough effects are likely to be irreversible. The shearing behaviour between  $\zeta_n$  and  $\zeta_i$  is dependent on the same conditions that produced the shear between  $\zeta_i$  and  $\zeta_n$  and cannot be influenced independently; but it can be regarded as a characteristic of the process that some modifications of surface pattern and indeed some of the characteristic features of marble patterns are likely to result from the two changes in shear direction. Figure 10 shows shear rate at the roll surface for  $\nu = 3$ ,  $U_1 = U_2$ ,  $h_n = 0.4$ , together with the cumulative shear, plotted against  $\zeta$ .

The means of producing uniquely distinctive patterns is usually kept secret. The relative striation susceptibilities of a range of components differing in both power-law flow constants give rise to a great complexity of pattern-making possibilities. Figure 11 shows log-log plastometry plots of six components of one particular coloured agglomerate of a filled thermoplastic. Curves (a), (e) and (f) are of similar slope  $\nu$  but show different specific fluidities. Curves (b) and (d) have a higher shear susceptibility but show intermediate fluidity and curve (c) crosses (b) and (d). These mixes differed only in pigments and in proportions of fillers (mainly wood flour).

Figure 12 shows the development of surface striations in a sheet which had been prepared with alternate stripes of two coloured components of different thicknesses and melt viscosities, running perpendicular to the flow axis. The rolls were stopped and opened simultaneously in order to release the samples. It is obvious from Figure 12 that the material did not adhere to the roll surface until the point A was reached. There is in fact considerable evidence for slippage of thermoplastics against metal surfaces, particularly under low pressures and temperatures and with mixes containing large proportions of fillers. The material used in the experiments was a mix of oxidized drying oil with about 60% of filler consisting of wood flour and pigments. Such binders

stick tenaciously to a cold steel surface, but have a very low viscosity against a hot one. Thus in some of the experiments it was found that the material had slipped continuously against the hot rolls, whereas there was evidence of a high shear rate in layers adjacent to the cold roll.

## OUTSTANDING PROBLEMS

The flow rate has been defined by equalizing roll speed and sheet speed at  $\zeta_n$ :  $Q = LUh_n = LUH_e$ . It is meaningless to attempt to define a new exit thickness which is greater due to elastic recovery, and at which the sheet speed equals the roll speed, because this redefines  $h_n$  and thus  $\zeta_n$  and  $\zeta_i$ ; and merely requires a smaller nip gap to achieve a given exit sheet thickness.

If we are concerned about the effect of elastic recovery (and it should be noted that most thermoplastics exhibit elastic recovery after shear deformation) we have to consider a situation in which the material leaves the rolls at a thickness greater than  $h_n$ , i.e.  $|\zeta_i| > |\zeta_n|$ , but where the mean speed of the sheet is lower than that of the roll surfaces. From Eq. (11), Appendix A, the minimum velocity when roll speeds are equal is obtained by putting  $y/h = 0$ , so that

$$\frac{u}{U} = 1 - (1 - h_n/h) \cdot \frac{\nu + 2}{\nu + 1}$$

For instance, if  $h_e = 1.25 h_n$  and  $\nu = 3$ ,  $u = 0.75U$ . This type of effect might occur due to strong adhesion of material to rolls, or due to recovery from normal stress differences in the extrudate. In the latter case the material has not moved into the next region of the theoretical pressure profile beyond  $-\zeta_n$  because the normal stress requiring dissipation is of elastic rather than viscous origin. The sheet has arrived at  $-\zeta_n$  unable to leave the roll surfaces because it is in tension. The present state of knowledge on normal stress effects should make possible a more comprehensive study of this aspect of the process.

Slippage in the inlet region is obviously an obstacle to a straightforward mathematical description of flow behaviour. In industrial technology this may not matter, since enough information can be obtained for practical purposes from simple theory and practice.

The attempted procuring of "strain profiles" has been described in the section on surface pattern. The section shown in Figure 12 showed profiles tallying reasonable well with the calculated ones for  $\nu = 3$  shown in Figure 13, but quite fortuitously. Most of the samples calendered showed adequately the striation effects near the sheet surface to explain the formation of patterns, but exhibited chevronny profiles (Figure 14) along their central plane. These

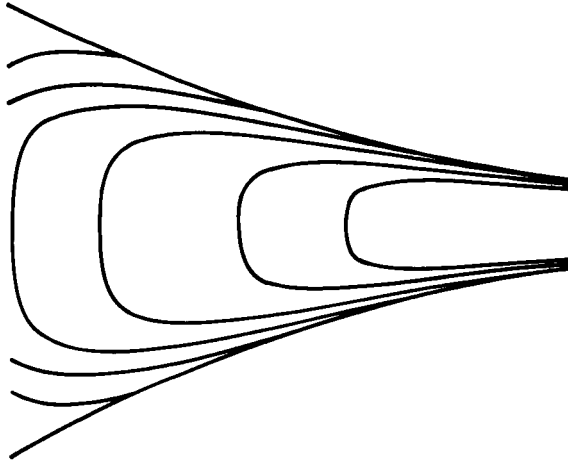


FIGURE 13 Calculated strain profiles for  $U_1 = U_2, \nu = 3$ .

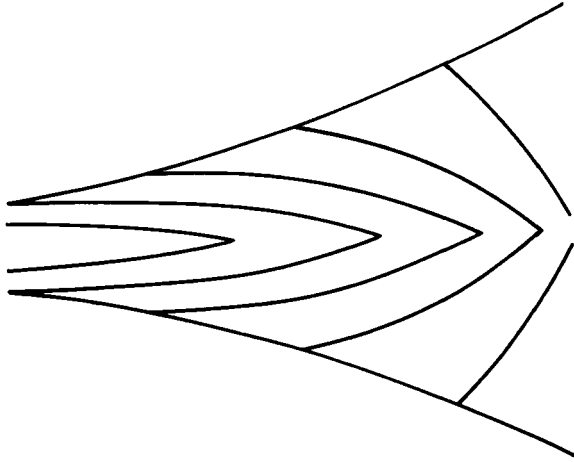


FIGURE 14 Observed  $V$  shaped profiles can be approximated theoretically only by putting  $\nu = 0$ .

cannot be explained in terms of viscous flow, and are probably due to the initial kinking of the leading edges of the samples on entering the nip. This had been noticed in earlier work with a larger calender. A refinement of the technique would present the striped samples as part of a larger sheet, so that a steady state could be reached before the experiment took place.

## Symbols

$e$	suffix denoting exit plane
$h$	half the gap between the rolls at any point along the z-axis
$i$	suffix denoting inlet plane
$n$	suffix denoting "neutral" plane, i.e. plane including pressure maximum
$o$	suffix denoting plane of the calender nip
$p$	pressure in the mass being calendered at any point along the z-axis
$t$	time
$u$	fluid velocity in z-direction
$y$	vertical distance from zero shear stress, measured towards upper roll
$z$	distance from nip plane contrary to flow direction
$C$	circumferential force at roll surface
$G$	pressure gradient $dp/dz$
$H$	total horizontal force on roll bearings
$K$	collection of terms from Eqs. (9) and (10), Appendix A
$L$	axial lengths of rolls wetted by calendered material
$Q$	volumetric flow rate of calendered material in z-direction
$R$	radius of roll
$U$	surface velocity of roll, faster $U_1$ , slower $U_2$
$V$	total vertical force on roll bearings
$\zeta$	$= Z/\sqrt{2Rh_0} = \sqrt{h/h_0} - 1$
$\gamma$	(gamma) amount of shear
$\dot{\gamma}$	shear rate $= dy/dt$
$\lambda$	(lambda) $= h_1/h_2$
$\nu$	(nu) exponent of shear stress in flow function
$\rho$	(rho) ratio of roll speeds $U_1/U_2$
$\sigma$	(sigma) shear stress
$\tau$	(tau) shear stress at roll surface
$\phi$	(phi) specific fluidity; shear rate and thus reciprocal viscosity at unit shear stress

## References

1. G. Ardichvili, *Kautschuk* **14**, 23 (1938).
2. D. D. Eley, *J. Pol. Sci.* **1**, 529 (1946).
3. R. E. Gaskell, *J. Appl. Mech.* **17**, 334 (1950).

4. E. B. Atkinson and H. A. Nancarrow, *Trans. Plast. Inst.*, Oct. 23 (1951).
5. J. T. Bergen and G. W. Scott, *J. Appl. Mech.* **18**, 101 (1951).
6. F. D. Dexter and D. I. Marshall, *S.P.J.*, April, 17 (1956).
7. P. P. Paslay, *J. Appl. Mech.* **24**, 602 (1957).
8. J. M. McKelvey, *Polymer Processing*, Wiley (1962).
9. J. R. A. Pearson, *Mechanical Principles of Polymer Melt Processing*, Pergamon (1966).

## Appendix A

### PRESSURE AND VELOCITY EQUATIONS, EQUAL ROLL SPEEDS

The power-law flow equation

$$\dot{\gamma} = du/dy = \phi \sigma^{\nu} = \phi (dp/dz)^{\nu} y^{\nu} \quad (6)$$

is used, a datum line  $y = 0$  having been defined as the line of zero shear rate. When  $U_1 = U_2$  the system is symmetrical. Integration of Eq. (6) gives

$$u = U - \phi G^{\nu} (h^{\nu+1} - y^{\nu+1}) / (\nu + 1) \quad (7)$$

because  $u = U$  where  $y = h$ .  $G = dp/dz$ ; for other nomenclature see Figure 1 and page 11.

The total rate of flow  $Q$  is given by

$$Q/2L = \int_0^h u \cdot dy = Uh - \phi G^{\nu} h^{\nu+2} / (\nu + 2) \quad (8)$$

Rearranging with  $y = z/\sqrt{2Rh_0}$ ,  $h/h_0 = 1 + \zeta^2$ , gives

$$\phi G^{\nu} = (\nu + 2) U \cdot \frac{h - h_n}{h^{\nu+2}} = (\nu + 2) \frac{U}{h_0^{\nu+1}} \left[ \frac{\zeta^2 - \zeta_n^2}{(1 + \zeta^2)^{\nu+2}} \right] \quad (9)$$

so that

$$G = \frac{dp}{dz} = K_1 \left[ \frac{\zeta^2 - \zeta_n^2}{(1 + \zeta^2)^{\nu+2}} \right]^{1/\nu} \quad (10)$$

Where at  $\zeta = \zeta_n$   $dp/dz = 0$  and  $\dot{\gamma} = 0$  at all  $y$  so that  $u = U = Q/2Lh_n$ . pressure gradient ( $dp/dz$ ) from Eq. (9) is shown plotted in Figure 2 for  $\nu = 4$ , thus eliminating  $\phi G^{\nu}$  from Eqs. (8) and (9).

## Appendix B

### BEARING LOADS AND DRIVE POWER

The vertical force  $V$  on the roll due to pressure on its surface is given by

$$V = \int_{z_1}^{z_2} p.L.dz \quad (12)$$

which can be written in the form

$$V = LK_1 2Rh_0 I_1(\zeta_1, \nu) \quad (13)$$

where  $K_1$  is from Eqs. (9) and (10) in Appendix A and  $I_1(\zeta_1, \nu)$  is the integral

$$\int_{\zeta_1}^{-\zeta_n} \zeta F(\zeta) d\zeta$$

There is a further load due to the vertical component of shear stress at the roll surface, which is small compared with that due to pressure and can be neglected.

The horizontal load  $H$  on the bearings is zero because

$$\int_{h_1}^{h_2} p.dh + \int_{z_1}^{z_2} \tau.dz = 0$$

where  $\tau$  is the surface shear stress  $Gh$ . The circumferential force  $C$  on the roll surface is given by

$$C = \int_{s_1}^{s_2} \tau.L.ds \quad (14)$$

where  $s$  is measured along the circumference of the roll. This can be written in the form

$$C = \sqrt{2Rh_0} L K_1 h_0 I_2(\zeta_1, \nu) \quad (15)$$

where it has been assumed that  $s \approx z$ .  $I_2(\zeta_1, \nu)$  is the integral

$$\int_{\zeta_1}^{-\zeta_n} (1 + \zeta^2) F(\zeta) d\zeta$$

Hence the ratio of total bearing load to the torque on one of the rolls is

$$\frac{V}{RC} = \sqrt{\frac{2}{Rh_0}} \cdot \frac{I_1}{I_2} \quad (16)$$

## Appendix C

### UNEQUAL ROLL SPEEDS

Considering the geometry of Figure 7

$$u_1 = U_1 - \phi G^v (h_1^{v+1} - y_1^{v+1}) / (v + 1) \quad (17)$$

and similarly for  $u_2$ . At  $y_1 = y_2 = 0$ ,  $u_1 = u_2$  so that

$$(U_1 - U_2)(v + 1) = \phi G^v (h_1^{v+1} - h_2^{v+1}) \quad (18)$$

Integrating (17) with its complement for  $u_2$  to give the volumetric flow rates, followed by adding the two flows, gives the flow rate per unit roll length

$$\frac{Q}{L} = \frac{Q_1 + Q_2}{L} = (U_1 + U_2)h_n = U_1 h_1 + U_2 h_2 - \phi G^v (h_1^{v+2} + h_2^{v+2}) / (v + 2) \quad (19)$$

Now let  $\rho = U_1/U_2$ ,  $\lambda = h_1/h_2$ ,  $h_1 + h_2 = 2h$ . Substituting for  $G$  from Eq. (18) then gives

$$1 + \rho\lambda + (1 + \rho)(1 + \lambda)h_n/2h = (\rho - 1) \cdot \frac{v + 1}{v + 2} \cdot \frac{\lambda^{v+2} + 1}{\lambda^{v+1} - 1} \quad (20)$$

This can be rearranged to

$$\frac{h_n}{2h} = \frac{1}{\rho + 1} + \frac{\rho - 1}{\rho + 1} \left[ \frac{\lambda/(\lambda + 1) - (v + 1)/(\lambda^{v+1} - 1)}{v + 2} \right] \quad (21)$$

which is a more convenient form for computation, since the  $\rho$  and  $\lambda$  functions have been separated.

Equation (19) can be written in the form

$$\frac{\phi G^v h_n^{v+1}}{2\bar{U}(v + 1)} = \frac{\rho - 1}{\rho + 1} \left[ \frac{(\lambda + 1)^{v+1}}{\lambda^{v+1} - 1} \right] \left( \frac{h_n}{2h} \right)^{v+1} \quad (22)$$

When calculating manually, values of  $\lambda$  are selected for chosen values of  $v$  and  $\rho$ , and  $h_n/2h$  values calculated from Eq. (21). From the values of  $h_n/h$ ,  $\zeta$  values for plotting are obtained via the relationship  $\zeta^2 = (h/h_n)(h_n/h_0) - 1$ , having selected a value for  $h_n/h_0$ . In manual computation and graphical integration to obtain pressure profiles it is necessary to choose a value of  $\zeta_n$ , so that  $\zeta_1$  is obtained as a result of the integration.